Bulletin of Mathematical Biology (2010) 72: 2139–2160
DOI 10.1007/s11538-010-9532-5

ORIGINAL ARTICLE

The Influence of Gene Expression Time Delays on Gierer–Meinhardt Pattern Formation Systems

S. Seirin Lee[a,*], E.A. Gaffney[b], N.A.M. Monk[c]

[a] *Graduate School of Environmental Sciences, Okayama University, Okayama 700-8530, Japan*
[b] *Centre for Mathematical Biology, Mathematical Institute, University of Oxford, Oxford OX1 3LB, UK*
[c] *School of Mathematical Sciences, University of Nottingham, Nottingham NG7 2RD, UK*

Received: 3 June 2009 / Accepted: 1 March 2010 / Published online: 23 March 2010

Abstract There are numerous examples of morphogen gradients controlling long range signalling in developmental and cellular systems. The prospect of two such interacting morphogens instigating long range self-organisation in biological systems via a Turing bifurcation has been explored, postulated, or implicated in the context of numerous developmental processes. However, modelling investigations of cellular systems typically neglect the influence of gene expression on such dynamics, even though transcription and translation are observed to be important in morphogenetic systems. In particular, the influence of gene expression on a large class of Turing bifurcation models, namely those with pure kinetics such as the Gierer–Meinhardt system, is unexplored. Our investigations demonstrate that the behaviour of the Gierer–Meinhardt model profoundly changes on the inclusion of gene expression dynamics and is sensitive to the sub-cellular details of gene expression. Features such as concentration blow up, morphogen oscillations and radical sensitivities to the duration of gene expression are observed and, at best, severely restrict the possible parameter spaces for feasible biological behaviour. These results also indicate that the behaviour of Turing pattern formation systems on the inclusion of gene expression time delays may provide a means of distinguishing between possible forms of interaction kinetics. Finally, this study also emphasises that sub-cellular and gene expression dynamics should not be simply neglected in models of long range biological pattern formation via morphogens.

Keywords Time delays · Gierer–Meinhardt system · Gene expression · Turing pattern formation

*Corresponding author.
E-mail addresses: seirin.lee@gmail.com; seirin@ems.okayama-u.ac.jp (S. Seirin Lee).

1. Introduction

Morphological pattern formation is a complex spatio-temporal process producing enormous diversity and yet with relatively few fundamental principles, typically utilising homologous and evolutionary conserved pathways. The primary mechanism driving morphogenesis is differential gene expression, which allows cells with identical DNA to differentially express proteins and thus to create, and respond to, heterogeneous environments in a context dependent manner. Consequently, gene expression in development requires rigorous coordination in both space and time; this is exerted by both long range signals, such as a diffusible-morphogen gradient, and short range signals as exemplified by cell-to-cell communication via signalling pathways. Examples of the latter occur with Notch signalling controlling the refinement of initial patterning events (Baron et al., 2002; Eldar et al., 2002; Harris et al., 2005). Long range signalling is of particular interest in that it allows the control of spatially heterogeneous expression of different target genes, providing the means of inducing and maintaining structure on lengthscales much larger than that of a cell.

However, while there are numerous examples of diffusible morphogens controlling developmental processes over large lengthscales, demonstrating whether morphogens *initiate* large scale symmetry breaking in developmental biology is much more elusive. The theoretical possibility of such self-organisation mechanisms was explored in a landmark paper by Turing (1952), which explicitly demonstrated that two diffusible morphogens could instigate a diffusively driven, symmetry breaking, bifurcation.

As recognised by Gierer and Meinhardt, and independently by Segel and Jackson, a fundamental property for instabilities in such systems is short range activation and long range inhibition (Gierer and Meinhardt, 1972; Koch and Meinhardt, 1994; Segel and Jackson, 1972). In the context of a biochemical interpretation, this requires a low diffusivity autocatalytic morphogen, the activator, and a high diffusivity, self-depleting morphogen, the inhibitor. If the activator also up-regulates the inhibitor, in combination with the inhibitor down-regulating the activator, a Turing instability is generally possible; this is referred to as a pure kinetics model, as exemplified by Gierer and Meinhardt's eponymous system. A Turing instability is also possible if the interaction between the activator and inhibitor is reversed, with the activator down-regulating the inhibitor, which in turn up-regulates the activator. This is a cross kinetics Turing model, a paradigm example of which is the Schnakenberg (1979) system.

The Turing instability mechanism has not only fascinated theoreticians. Though it has remained elusive, it has been explored, postulated, or implicated in a number of developmental biology settings. These include: vertebrate limb development (Miura and Maini, 2004; Miura and Shiota, 2000), avian feather bud formation (Jung et al., 1998), embryonic feather branching (Harris et al., 2005), zebrafish mesendoderm induction (Krezel, 2003), and the amplification of embryonic left-right symmetry breaking events (Juan and Hamada, 2001). However, despite an enormous literature on how diffusible morphogens may initiate spatial patterning, there are remarkably few investigations of the temporal aspects of these biological pattern formation mechanisms (Miura and Maini, 2004; Page et al., 2007; Veflingstad et al., 2005). Nonetheless, developmental processes can proceed at rapid, yet well defined, rates which is indicative of tight temporal control, as exemplified by observations of the development of the zebrafish bodyplan (Kimmel et al., 1995).

In addition, modern experimental interrogations of suspected morphogen based pattern formation systems, such as Nodal and Lefty zebrafish mesendodermal induction, utilise *in situ* hybridisation (Chen and Schier, 2002; Jing et al., 2006; Krezel, 2003). This explicitly highlights local concentrations of specific mRNA transcripts and thus provides an indication of the rates of transcription of target genes, and emphasises the role of gene expression in morphogenesis. The fact that gene expression time delays are difficult to manipulate experimentally ultimately entails that it is difficult to ascertain how they influence biological pattern formation, and hence modelling studies are particularly informative. However, the influence of gene expression on morphogen based pattern formation systems has only been considered in one single investigation for a specific form of reaction kinetics (Gaffney and Monk, 2006). Nonetheless, this study highlighted that gene expression had a profound effect on predicted patterning timescales, and thus greatly influences the temporal control that could be exerted via morphogens on large scale pattern formation.

The reason for this profound influence lies in the classical molecular biology of gene expression itself. Signals instigating changes in gene expression are transduced via tightly regulated biochemical cascades which ultimately result in protein production. This latter event proceeds via the transcription of nuclear DNA, forming mRNA, which in turn is translated into protein within the cytosol, consequently altering cellular function, metabolism, and importantly intercellular signalling, thus ultimately creating a feedback loop. However, signal transduction, gene transcription and mRNA translation take time; consequently, the feedback is delayed. Empirical estimates for the magnitudes of transcriptional and translational timescales, while dependent on the size of the genomic sequence, are estimated to be approximately from 10 minutes to several hours (Lewis, 2003; Tennyson et al., 1995). Critically, the previous study (Gaffney and Monk, 2006) observed that even these relatively small gene expression delays substantially amplify patterning lags, thus demonstrating the potential for gene expression dynamics to exert enormous temporal influence on pattern formation.

An important question that arises is whether the observations of this earlier paper are generally representative, given the focus on particular choice of morphogen interaction kinetics, the Schnakenberg system. On the one hand, if the Schnakenberg system is representative, it is clear that gene expression time delays are an important consideration in the temporal control of putative Turing-type biological self-organisation models. On the other, if alternative Turing-type models behave radically differently on the introduction of gene expression time delays, then there is a possible means of differentiating between or eliminating certain choices of interaction kinetics.

Given Schnakenberg kinetics are a paradigm form of cross kinetics, we therefore focus on pure kinetics, using Gierer and Meinhardt's model as this is a classic and common example. The distinction between cross and pure kinetics is rarely made in the literature as these two types of Turing pattern formation models have previously been observed to behave similarly with both generating the Turing instability bifurcation (Murray, 1993). However, this need not be true in the presence of gene expression time delays. For example, in contrast to the Schnakenberg system, negative feedback loops exist within the morphogen interactions of Gierer and Meinhardt's model. This suggests there may be the possibility of combinations of negative feedback loops and time delays inducing oscillatory behaviour not seen in the delayed Schnakenberg model considered in the previous study. Furthermore, while threshold or hysteretic cell responses could be designed to

yield patterns in the presence of temporal oscillations with spatially heterogeneity, such pattern formation would have a characteristic signature of oscillating in-situ hybridisation profiles; this would be quite distinct from the standard Turing model. Whether such behaviour emerges will therefore be a fundamental focus of this investigation.

A further question is the sensitivity to the modelling details of the time delay at the sub-cellular level. An implicit assumption in Turing morphogen models of biological pattern formation is that the detailed sub-cellular dynamics can be summarised via simple interactions of gene products. This, however, is only rarely explored; one explicit example is recent work by Rauch and Millonas (2004) which has shown that the inclusion of simple intra-cellular dynamics allows patterning for morphogen pairs with equal diffusive lengthscales. This observation is important in that it suggests a mechanism for morphogen patterning without the need for short-range activation and long range inhibition, which in turn emphasises the potential importance of sub-cellular dynamics. In addition, modelling gene expression time delays is, in effect, explicitly considering the influence of a critical aspect of the sub-cellular dynamics, though this interpretation was not explored in-depth for the previous study (Gaffney and Monk, 2006). Thus, we shall also investigate whether different possible forms of the sub-cellular gene expression dynamics, which reduce to the Gierer–Meinhardt model in the absence of time delays, result in radically different system behaviour.

In summary, we will investigate the effects of gene expression time delays in the Gierer–Meinhardt model, which is an exemplar two component, reaction diffusion pattern formation model with pure kinetics. Our aim is to assess whether gene expression time delays induce radically different spatial or temporal behaviour for exemplar models of morphogen pattern formation differing only in the details of the gene product kinetics or the details of the sub-cellular dynamics modelling gene expression.

2. Models

2.1. The generic Turing model; pure and cross kinetics

The Turing model assumes the presence of two interacting and diffusing morphogens, which in one spatial dimension can be represented by the following equations (Murray, 1993):

$$\frac{\partial U}{\partial t} = D_U \frac{\partial^2 U}{\partial x^2} + f(U, V), \qquad \frac{\partial V}{\partial t} = D_V \frac{\partial^2 V}{\partial x^2} + g(U, V). \tag{1}$$

We have, without loss of generality, that U and V respectively denote the concentration of the activator and the inhibitor. The short range influence of the activator entails that it has a lower diffusivity and hence $D_U < D_V$; to avoid extreme parameter fine tuning in the requirements for pattern initiation, one in fact requires $D_U \ll D_V$ (Baker et al., 2008). These equations are supplemented with boundary conditions, which are usually, but not necessarily, zero flux.

Typically, the choice of $f(U, V)$, $g(U, V)$ is such that there is only a single homogeneous steady state as the dynamics associated with multiple steady states, for example bistable switching (Varea et al., 2007), is not relevant in ensuring the initiation and stability of biological self-organisation. The choice of pure kinetics entails further restrictions

on the choice of the functions f and g. With $(U_*,\ V_*)$ denoting the homogeneous steady state and $f_U,\ f_V,\ g_U,\ g_V$ denoting partial derivatives, pure kinetics are such that

$$\begin{pmatrix} f_U(U_*, V_*) & f_V(U_*, V_*) \\ g_U(U_*, V_*) & g_V(U_*, V_*) \end{pmatrix} \sim \begin{pmatrix} + & - \\ + & - \end{pmatrix}, \tag{2}$$

as this gives the required activator and inhibitor interactions if pattern should initiate from fluctuations about the homogeneous steady state. The signs of the off-diagonals are reversed for cross kinetics.

2.2. *The Gierer–Meinhardt system with no gene expression time delay*

In the absence of gene expression time delays, we use Gierer–Meinhardt kinetics (Gierer and Meinhardt, 1972). Such models can be considered to be a very simplified representation of the interaction dynamics seen in many morphogen systems. One example is Nodal signalling, where Nodal protein induces Nodal production but is inhibited by Lefty as part of a negative feedback loop (Chen and Schier, 2002; Iratini et al., 2002; Schier, 2003). Numerous complications that occur with Nodal and Lefty or in other signalling systems, such as the influence of co-receptors and secondary inhibitors (Schier, 2003), are neglected so that our focus is the core morphogen interactions.

Gierer and Meinhardt's model is

$$\begin{aligned} \frac{\partial U}{\partial t} &= D_U \frac{\partial^2 U}{\partial x^2} + k_1 - k_2 U + k_3 \frac{U^2}{V}, \\ \frac{\partial V}{\partial t} &= D_V \frac{\partial^2 V}{\partial x^2} + k_4 U^2 - k_5 V, \end{aligned} \tag{3}$$

where $k_1, \ldots, k_5$ are positive definite and dictate the production rate, the decay rates and rate of gene product interactions of the morphogens.

In addition to basal rates, activator production proceeds by an autocatalytic interaction between two activator molecules, the rate of which is down-regulated by the inhibitor while inhibitor synthesis proceeds via activator cross catalysis. A biochemical interpretation of the form of the activator and inhibitor interactions can be summarised by

$$U + U \xrightarrow{k_3/V} 3U, \tag{4}$$

$$U + U \xrightarrow{k_4} 2U + V, \tag{5}$$

where k_3/V and k_4 are reaction rates; the V dependent reaction rate crudely models the inhibitor's tendency to down-regulate activator production.

2.3. *The Gierer–Meinhardt system with gene expression time delays*

The first step in the mechanism by which extracellular morphogens induce gene expression is by binding to cell surface receptors which instigates signal transduction via protein- and lipid-mediated kinase cascades. These, in turn, control levels of protein production via gene expression (Alberts et al., 2002). A key regulatory mechanism controlling signal

transduction, and thus inter-cellular signalling is the endocytosis of cell surface receptors and their bound ligands. A dominant view has emerged that ligand-induced receptor tyrosine kinase endocytosis is primarily a mechanism for attenuating receptor mediated signals (Beguinot et al., 1984; Sorkin and von Zastrow, 2002; Stoscheck and Carpenter, 2002; Wells et al., 1990). However, the detection of protein interactions in endosomes is supporting a growing body of evidence that signal transduction may be instigated from endosomal membranes such as TGF-β signalling in vertebrate cells and Dpp signalling in *Drosophila* (Entchev et al., 2000; Fischer et al., 2006; Piddini and Vincent, 2003; Roy and Wrana, 2005; Sorkin and von Zastrow, 2002).

Consequently, below, we shall typically adopt two models representing two extremes. In the first model, signal transduction for the production of morphogen is solely induced by reversible ligand binding at the cell surface. For the second model, all such signal transduction is assumed to proceed via internalised ligand. Additional models are briefly considered with combinations of these mechanisms of signal transduction. All models also have an independent ligand-induced receptor endocytosis, which effectively results in ligand decay. Clearly, these are not unique possibilities. Nonetheless, by exploring the predictions of these models we can highlight whether or not the details of the gene expression dynamics are important when considering morphogen based simulations of biological pattern formation.

Finally, we note that there are many simplifications in the consideration of the molecular level dynamics for either model. For example, we neglect the possibility of ligand recycling, which would lead to a system with two types of time delays in the morphogen dynamics, one due to gene expression and the other due to recycling. We do not consider the possibility of low copy number dynamics and the consequent stochasticity. As a final example of biology neglected in our modelling, the above Gierer Meinhardt model, Eq. (3), does not consider receptor dynamics, and thus effectively assumes an inexhaustible supply of receptors.

2.3.1. Model I

In addition to a constant production of activator, we have activator and inhibitor decay, for example via an independent ligand-induced receptor endocytosis. We also have that two molecules of activator can reversibly bind a receptor to induce, ultimately, the production of a molecule of inhibitor. However, this production is delayed by a time, τ. Similarly, we have that two molecules of activator can reversibly bind a receptor to induce, ultimately, the production of an additional molecule of activator though again this production is delayed by a time, τ. For simplicity, we assume throughout that the time delay of both gene expression events is the same and constant.

This representation of gene expression dynamics, including the antagonism of activator production by the inhibitor, is summarised in both Fig. 1 and in the following reaction scheme:

$$\mathbf{U}_{\mathbf{t}*-\tau} + \mathbf{U}_{\mathbf{t}*-\tau} \xrightarrow{k_3/V_{t*-\tau}} \mathbf{2U}_{\mathbf{t}*-\tau} + \mathbf{U}_{\mathbf{t}*}, \tag{6}$$

$$\mathbf{U}_{\mathbf{t}*-\tau} + \mathbf{U}_{\mathbf{t}*-\tau} \xrightarrow{k_4} \mathbf{2U}_{\mathbf{t}*-\tau} + \mathbf{V}_{\mathbf{t}*}, \tag{7}$$

where $\mathbf{U_s}, \mathbf{V_s}$, respectively, denote the activator and inhibitor proteins at time s. Thus, morphogen induced protein production at time t is dictated by interactions at time $t - \tau$,

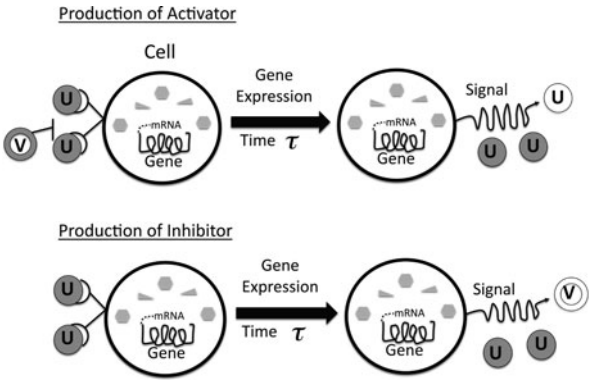

Fig. 1 A representation of Model I. The *upper* figure is a representation of the auto-catalytic production of activator. The *gray circles* labelled by U represent extracellular molecules of the activator. Via reversible ligand binding, these induce a signal, subject to extracellular inhibitor antagonism, as represented by the *circle* labelled by V and possessing a gray annulus. The result of this signal, after a time delay τ, is the production of an activator molecule, represented by the *white circle* labelled with U. In the absence of other reactions, the signal inducing molecules are still present, as depicted on the *right* of the *upper* graphic. In the *lower* figure, activator induced production of inhibitor is represented, again with no ligand internalisation for the induction of signal. The resulting molecule of inhibitor is represented on the *right* of the *lower* graphic by the *circle* labelled by V, with a *white* surrounding annulus.

giving the equations

$$\begin{aligned}\frac{\partial U}{\partial t} &= D_1\frac{\partial^2 U}{\partial x^2} + k_1 - k_2 U(x,t) + k_3\frac{U^2(x,t-\tau)}{V(x,t-\tau)},\\ \frac{\partial V}{\partial t} &= D_2\frac{\partial^2 V}{\partial x^2} + k_4 U^2(x,t-\tau) - k_5 V(x,t).\end{aligned} \tag{8}$$

Relabel the dimensional time coordinate, time delay, and spatial coordinate by t_{dim}, τ_{dim}, and x_{dim}; also let L denote the dimensional domain length. With a timescale T_s, the non-dimensionalisation

$$t = t_{\mathrm{dim}}/T_s, \qquad \tau = \tau_{\mathrm{dim}}/T_s, \qquad x = x_{\mathrm{dim}}/L, \qquad \gamma = T_s k_5, \qquad D = T_s D_2/L^2,$$
$$a = k_1 k_4/k_3 k_5, \qquad b = k_2/k_5, \qquad u = (k_4/k_3)U, \qquad v = \left(k_4 k_5/k_3^2\right)V,$$

reduces Model I to the form

$$\begin{aligned}\frac{\partial u}{\partial t} &= \epsilon^2 D\frac{\partial^2 u}{\partial x^2} + \gamma\left\{a - bu(x,t) + \frac{u^2(x,t-\tau)}{v(x,t-\tau)}\right\},\\ \frac{\partial v}{\partial t} &= D\frac{\partial^2 v}{\partial x^2} + \gamma\left\{u^2(x,t-\tau) - v(x,t)\right\},\end{aligned} \tag{9}$$

where $\epsilon^2 = D_1/D_2$ and the non-dimensionalised spatial domain is given by $x \in [0,1]$.

2.3.2. Model II

The difference with Model II is that morphogen production proceeds via signal transduction processes that require ligand internalisation. Thus morphogen production is sum-

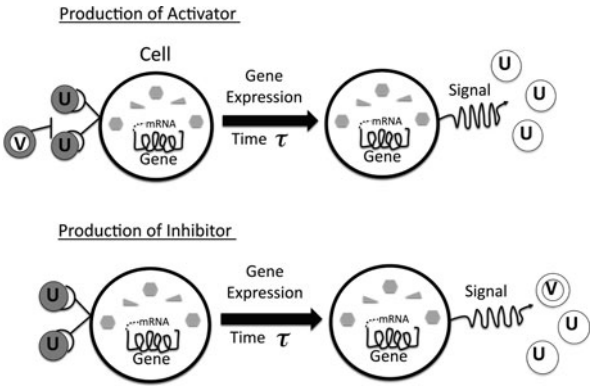

Fig. 2 A representation of Model II. The *upper* figure is a representation of the auto-catalytic production of activator. Once more, the *gray circles* labelled by U represent extracellular molecules of the activator. Subject to inhibitor antagonism, as represented by the *circle* labelled by V and possessing a *gray* annulus, activator molecules bind to surface receptors, and are internalised. These internalised molecules ultimately instigate a signal resulting in the production of three activator molecules, though with a time delay τ. This is represented by the *white circles* labelled with U on the *right* of the *upper* graphic. In the *lower* figure, activator induced production of inhibitor is represented, again with ligand internalisation. The resulting molecules of activator and inhibitor and represented on the *right* of the *lower* graphic by *white circles*, labelled by U and V, respectively, with the icon for the inhibitor also surrounded by a *white* annulus.

marised in Fig. 2 and by the following reaction scheme:

$$\mathbf{U}_{t*-\tau} + \mathbf{U}_{t*-\tau} \xrightarrow{k_3/V_{t*-\tau}} \mathbf{3U}_{t*}, \tag{10}$$

$$\mathbf{U}_{t*-\tau} + \mathbf{U}_{t*-\tau} \xrightarrow{k_4} \mathbf{2U}_{t*} + \mathbf{V}_{t*}. \tag{11}$$

With the definition $c = 2k_3/k_5$, writing down the equations corresponding to the above reaction scheme and performing a suitable non-dimensionalisation, essentially identical to that of Model I, yields the non-dimensionalised Model II:

$$\begin{aligned}\frac{\partial u}{\partial t} &= \epsilon^2 D\frac{\partial^2 u}{\partial x^2} + \gamma\left\{a - bu(x,t) + 3\frac{u^2(x,t-\tau)}{v(x,t-\tau)} - 2\frac{u^2(x,t)}{v(x,t)}\right.\\ &\qquad \left. + c\left\{u^2(x,t-\tau) - u^2(x,t)\right\}\right\},\\ \frac{\partial v}{\partial t} &= D\frac{\partial^2 v}{\partial x^2} + \gamma\left\{u^2(x,t-\tau) - v(x,t)\right\}.\end{aligned} \tag{12}$$

2.3.3. Models III and IV

Model III is analogous to Models I and II except that its non-linear morphogen production is based upon reactions (6) and (11); thus, inhibitor production proceeds via ligand internalisation but the autocatalytic production of activator is instigated by reversible ligand binding at the cell surface. Model IV, with non-linear morphogen production based on reactions (7) and (10), is analogous and both Models III and IV are very briefly considered below in explorations of the influence of sub-cellular dynamics on patterning.

2.3.4. The saturation of activator induced activator production

A variation of Gierer and Meinhardt's model that we shall also briefly consider below incorporates the saturation of activator induced activator production, as may occur with a limited receptor supply. This is modelled using Gierer and Meinhardt's (1972) suggestion for activator production saturation whereby

$$k_3\frac{U^2}{V}\to k_3\frac{U^2}{[(1+kU^2)V]}$$

in Eq. (3), with $k\geq 0$. Thus, the activator production in the reaction scheme (4) generalises to

$$U+U\xrightarrow{k_3[(1+kU^2)V]^{-1}}3U; \tag{13}$$

hence the presence of saturating activator induced activator production can be incorporated into the non-dimensionalised versions of Models I–IV via the replacement

$$\frac{u^2}{v}\to\frac{u^2}{(1+\kappa u^2)v},$$

where $\kappa=kk_3^2/k_4^2$. Thus, in Model I, for example the evolution equation for $u(x,t)$ becomes

$$\frac{\partial u}{\partial t}=\epsilon^2D\frac{\partial^2u}{\partial x^2}+\gamma\left[a-bu(x,t)+\frac{u^2(x,t-\tau)}{[1+\kappa u^2(x,t-\tau)]v(x,t-\tau)}\right], \tag{14}$$

and the equation for the inhibitor, v is unchanged. Unless explicitly specified, $k=\kappa=0$ below and the saturation of activator induced activator production is not considered.

2.3.5. Boundary conditions

Zero flux boundary conditions are imposed; for the non-dimensionalised models this requires

$$\frac{\partial u}{\partial x}=\frac{\partial v}{\partial x}=0\quad\text{at } x=0,1. \tag{15}$$

2.3.6. Initial conditions

We consider initial conditions which are perturbations of the unique homogeneous steady state, denoted (u_*,v_*). In detail, for $t\in[0,\tau]$, we typically report results for two choices of perturbation:

$$\textbf{IC1}\colon u(x,t)=u_*+E_a\phi_1(x),\quad v(x,t)=v_*+E_b\phi_2(x), \tag{16}$$

$$\begin{aligned}\textbf{IC2}\colon u(x,t)&=\big(u_*+E_a\phi_1(x)\big)\big(1+\delta\cos\big(\pi t/(2\tau)\big)\cos(\pi x)\big),\\ v(x,t)&=\big(v_*+E_b\phi_1(x)\big)\big(1+\delta\cos\big(\pi t/(2\tau)\big)\cos(\pi x)\big),\end{aligned} \tag{17}$$

where $E_a, E_b, \delta\ll 1$ dictate the overall size of the perturbation and the functions $\phi_1(x)$, $\phi_2(x)$ are given by

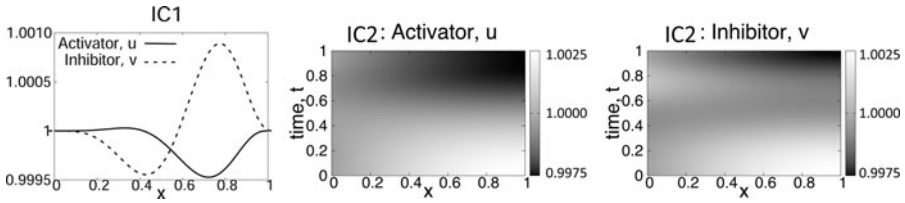

Fig. 3 The first, *left-hand*, plot depicts initial conditions IC1 with $E_a = 1.25\text{e}{-}03$ and $E_b = 6\text{e}{-}03$. The remaining two plots illustrate an example of initial condition IC2 with the same values of E_a, E_b, with $\delta = 2.5\text{e}{-}03$ and $\tau = 1$. The model parameters are such that the homogeneous steady state, (u_*, v_*), is equal to (1.0, 1.0).

$$\begin{aligned}\phi_1(x) &= x^5\big(1-x^2\big)\big(-170.6666682x^3 + 412.4444479x^2\\ &\quad - 312.8888910x + 71.1111113\big),\\ \phi_2(x) &= x^5\big(1-x^2\big)\big(-130.8444445x^3 + 337.0666669x^2\\ &\quad - 281.6000002x + 75.3777778\big).\end{aligned}$$

The precision of the coefficients simply ensure that zero flux boundary conditions are satisfied to within negligible error to avoid the mathematical complications that would arise if the boundary and initial conditions were incompatible. Examples of the initial conditions are illustrated in Fig. 3.

2.3.7. Reference parameter values

In Tables 1 and 2, we specify representative reference parameter values for the simulations below. Note the invariance of the non-dimensionalised equations with respect to the transformation $L \to \psi L$, $T_s \to \psi^2 T_s$ entails that all solutions are also valid on increasing the lengthscale by ψ and the timescale by ψ^2. Consequently, the non-dimensionalised parameters values and solutions below in fact correspond to one parameter families of dimensional solutions.

3. Results

3.1. Linearised equations for Models I and II

We briefly consider a linear analysis of the delay equations for both Model I and Model II. Denote the homogeneous steady state solution by (u_*, v_*) and substitute the Fourier expansion

$$\begin{pmatrix} u \\ v \end{pmatrix} = \begin{pmatrix} u_* \\ v_* \end{pmatrix} + \eta \sum_{n=1}^{\infty} A_n(t)\cos(n\pi x), \tag{18}$$

with $A_n(t) = (u_n(t), v_n(t))^T$ into either Eqs. (9) or (12). We also incorporate the possibility of saturation in activator induced activator production below, and thus in general $\kappa \geq 0$

Table 1 Parameter sets for Model I, which is summarised by Eq. (9), and Model II, summarised by Eq. (12). The physical domain size is taken to be 10^{-2} cm, which is approximately 10 cell lengths. The non-dimensionalised parameter sets I and II induce spatial patterns with one and two modes in the non-delayed Gierer–Meinhardt system (3). The gene expression time delays considered are between 2 minutes and 36 minutes. Note these parameters also correspond to a family of dimensional solutions, as detailed in Section 2.3.7

Parameter	Value
Physical domain size (L, cm)	10^{-2}
Diffusivity of the inhibitor (D_2, cm^2/sec)	10^{-6}
Ratio of diffusion coefficient (ϵ^2)	10^{-3}
Dimensional time scale (T_s, seconds)	100
Non-dimensionalised parameters	Set I
Diffusivity of the inhibitor (D)	1.0
Base production rate of the activator (a)	0.128
Decay rate of the activator (b)	0.667
$c = 2k_3/k_5$	42.667
Reaction rate ($\gamma = T_s k_5$)	0.75
Activator Induced Saturation ($\kappa = kk_3^2/k_5^2$)	0.1
Non-dimensional gene expression time delay (τ)	{0.0, 1.2, 1.3, 1.8, 8.4}
Dimensional gene expression time delay (min)	{0.0, 2.0, 2.2, 3.0, 14}
Non-dimensionalised parameters	Set II
Diffusivity of the inhibitor (D)	1.0
Base production rate of the activator (a)	0.004
Decay rate of the activator (b)	0.02
$c = 2k_3/k_5$	0.04
Reaction rate ($\gamma = T_s k_5$)	5.0
Activator Induced Saturation ($\kappa = kk_3^2/k_5^2$)	0
Non-dimensional gene expression time delay (τ)	{0.0, 3.6, 7.2, 8.4, 14.4, 21.6}
Dimensional gene expression time delay (min)	{0, 6, 12, 14, 24, 36}

for the linear analysis. Thus, we have at leading order in η that

$$\frac{d}{dt}A_n(t) = -n^2\pi^2 D\begin{pmatrix}\epsilon^2 & 0\\ 0 & 1\end{pmatrix}A_n(t) + \gamma\begin{pmatrix}F_1 & F_2\\ 0 & -1\end{pmatrix}A_n(t) + \gamma\begin{pmatrix}G_1 & G_2\\ G_3 & 0\end{pmatrix}A_n(t-\tau), \tag{19}$$

where, for Model I, we have

$$(F_1, F_2) = (-b, 0), \qquad (G_1, G_2, G_3) = \left(\frac{2u_*}{(1+\kappa u_*^2)v_*}, -\frac{u_*^2}{(1+\kappa u_*^2)v_*^2}, 2u_*\right),$$

and for Model II

$$(F_1, F_2) = -\left(b + \frac{4u_*}{(1+\kappa u_*^2)v_*} + 2cu_*, \frac{-2u_*^2}{(1+\kappa u_*^2)v_*^2}\right),$$

$$(G_1, G_2, G_3) = \left(\frac{6u_*}{(1+\kappa u_*^2)v_*} + 2cu_*, \frac{-3u_*^2}{(1+\kappa u_*^2)v_*^2}, 2u_*\right).$$

Table 2 Further parameter sets for Model I, which is summarised by Eq. (9), and Model II, summarised by Eq. (12). The physical domain size is taken to be $\sqrt{10} \times 10^{-2}$ cm, which is approximately 30 cell lengths and a different spatial scale from Table 1. The non-dimensionalised parameter set III is composed of kinetic parameter values which induce mode eight spatial patterns, that is four stripes, in the non-delayed system given by Eqs. (3). The timescale is the same as the earlier parameter sets and the gene expression time delays considered are between 3 minutes to 14 minutes. Note these parameters also correspond to a family of dimensional solutions, as detailed in Section 2.3.7

Parameter	Value
Physical domain size (L, cm)	$\sqrt{10} \times 10^{-2}$
Diffusivity of the inhibitor (D_2, cm^2/sec)	10^{-6}
Ratio of diffusion coefficient (ϵ^2)	10^{-3}
Dimensional time scale (T_s, seconds)	100
Non-dimensionalised parameters	Set III
Diffusivity of the inhibitor (D)	10^{-1}
Production rate of the activator (a)	0.0075
Decay rate of the activator (b)	0.05
$c = 2k_3/k_5$	0.1
Reaction rate ($\gamma = T_s k_5$)	8.0
Activator Induced Saturation ($\kappa = kk_3^2/k_5^2$)	0
Non-dimensional gene expression time delay (τ)	{0.0, 1.8, 3.6, 7.2, 8.4}
Dimensional gene expression time delay (min)	{0, 3, 6, 12, 14}

3.1.1. Analytical observations

A straightforward generalisation of the calculations presented by Gaffney and Monk (2006) shows that the linearised equations do not admit temporal oscillations at the Turing symmetry-breaking when increases in the domain size drive a bifurcation away from the homogeneous steady state, despite the presence of time delays. Further analytical details of the linearised equations are briefly considered in Appendix A, where it is shown that the patterning lag diverges as the time delay tends to infinity. This suggests patterning may be absent or retarded as the time delay increases and further motivates explorations of the patterning lag below.

3.1.2. Numerical results in the linearised system

Typical results from numerical simulations based on Heun's method (Morton and Mayers, 1994), though with the incorporation of delays, are depicted in Fig. 4 for the $n = 2$ mode of the linearised equations (19) with no saturation of activator induced activator production ($\kappa = 0$). The initial conditions are small, constant perturbations of the homogeneous steady state and parameter set II of Table 1 is used. Note that oscillations are never observed and the large time asymptote of the linear solution always diverges.

With $S_I^{\mathrm{Lin}}(\tau)$, $S_{II}^{\mathrm{Lin}}(\tau)$ respectively denoting the timescale for this linearised solution of Model I and Model II to leave a suitably small neighbourhood of the homogeneous steady state, we consistently find that

$$\frac{dS_I^{\mathrm{Lin}}}{d\tau} \ll \frac{dS_{II}^{\mathrm{Lin}}}{d\tau}.$$

We thus have the prediction that the temporal control of patterning in Model II is much more sensitive to fluctuations in the gene expression time delay, at least according to linear

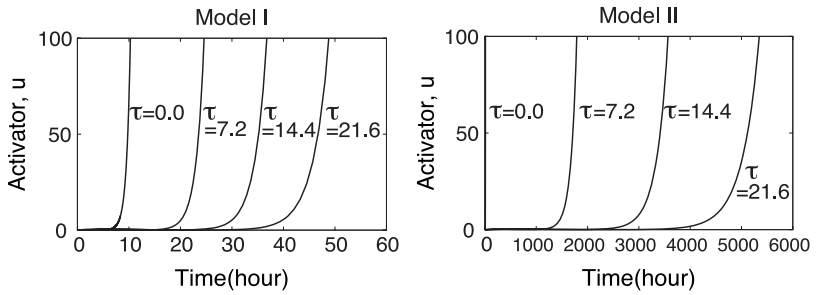

Fig. 4 Numerical predictions of the amplitude for the $n = 2$ mode of the activator concentration, as predicted by the linearised system (19) of Model I and II with no saturation of activator induced activator production ($\kappa = 0$). The non-dimensional parameters are given by set II of Table 1, though with non-dimensional delays of $\tau \in \{0.0, 7.2, 14.4, 21.6\}$. Note that in the *right-hand* figure the *curve* for $\tau = 0.0$ is indistinguishable from the *vertical axis* due to the time scale of the patterning lag.

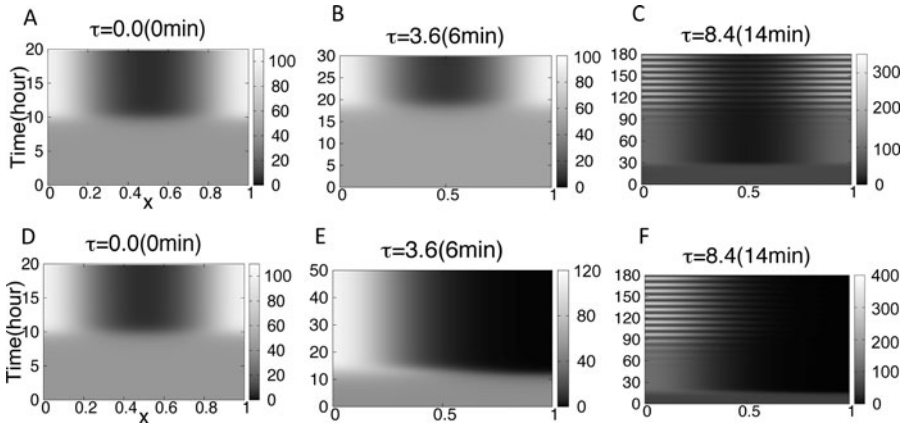

Fig. 5 Model I. In this and each subsequent analogous figure the greyscale represents the non-dimensionalised concentration of the activator, the *horizontal axis* is the non-dimensionalised spatial coordinate and the *vertical axis* is time, which has been rescaled to units of hours. The *first row* corresponds to parameter set II of Table 1 for initial conditions IC1, as given by Eq. (16) with $E_a = 1.25\text{e}{-03}$ and $E_b = 6\text{e}{-03}$. The *second row* corresponds to the same parameter values but with the initial conditions IC2 with $\delta = 2.5\text{e}{-03}$, as given by Eq. (17).

theory. Also, given $S_I^{\text{Lin}}(0) = S_{II}^{\text{Lin}}(0)$ by construction, linear theory also indicates that the patterning lag in Model II is much greater. Similar results, not shown, are obtained for more general initial conditions.

3.2. Numerical results for Models I and II

The numerical methods used here and also below are detailed in Appendix B. In this section, we present results for numerical simulations using the parameter sets listed in Tables 1, 2, and with the initial conditions IC1 and IC2, as defined by Eqs. (16) and (17). In Figs. 5–8, the greyscale plots depict the non-dimensionalised activator concentration

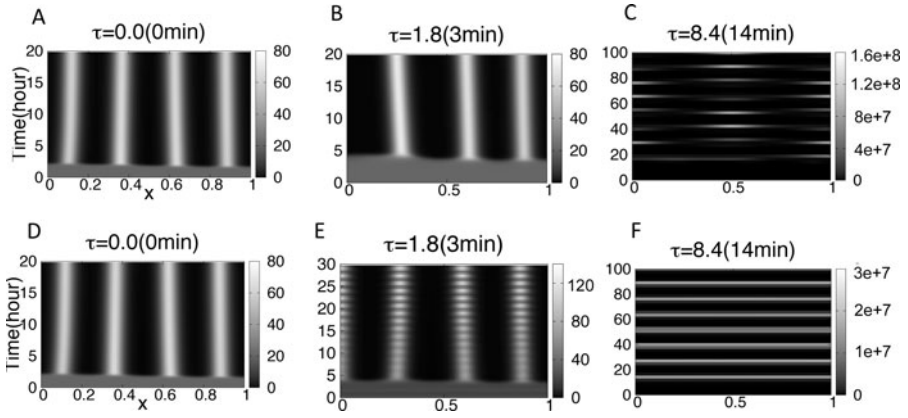

Fig. 6 Model I. The greyscale represents the non-dimensionalised concentration of the activator, the *horizontal axis* is the non-dimensionalised spatial coordinate and the *vertical axis* is time, which has been rescaled to units of hours. The parameters are given by set III of Table 2. In the *first row*, we have IC1 initial conditions, as defined by Eq. (16), for $E_a = 1.25\text{e}{-03}$ and $E_b = 6\text{e}{-03}$. In the *second row*, the IC2 initial conditions are used, as defined by Eq. (17) with $\delta = 2.5\text{e}{-03}$, for the same parameter values.

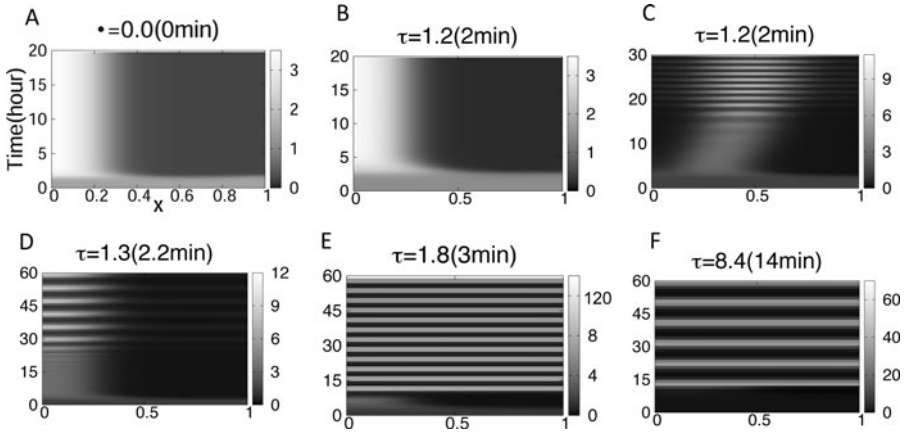

Fig. 7 Model I with the saturation of activator induced activator production. The greyscale represents the non-dimensionalised concentration of the activator, the *horizontal axis* is the non-dimensionalised spatial coordinate and the *vertical axis* is time, which has been rescaled to units of hours. With the exception of plot C, Parameter set I in Table 1 is used with initial conditions IC1, as given by Eq. (16), where $E_a = 1.25\text{e}{-03}$, $E_b = 6\text{e}{-03}$ and, to three significant figures, $(u_*, v_*) = (1.44, 2.06)$. For plot C, the only difference is that $E_a = 1.25\text{e}{-04}$ within the initial conditions.

and the horizontal axis is the non-dimensionalised spatial coordinate of the domain. The vertical axis is time, which has been rescaled to units of hours noting the timescale T_S is 100 seconds; this choice of presentation assists in emphasising the timescale of pattern formation compared to typical estimates of the gene expression time delay. As typical for pure kinetics, peaks, and troughs of the inhibitor are in-phase with the activator.

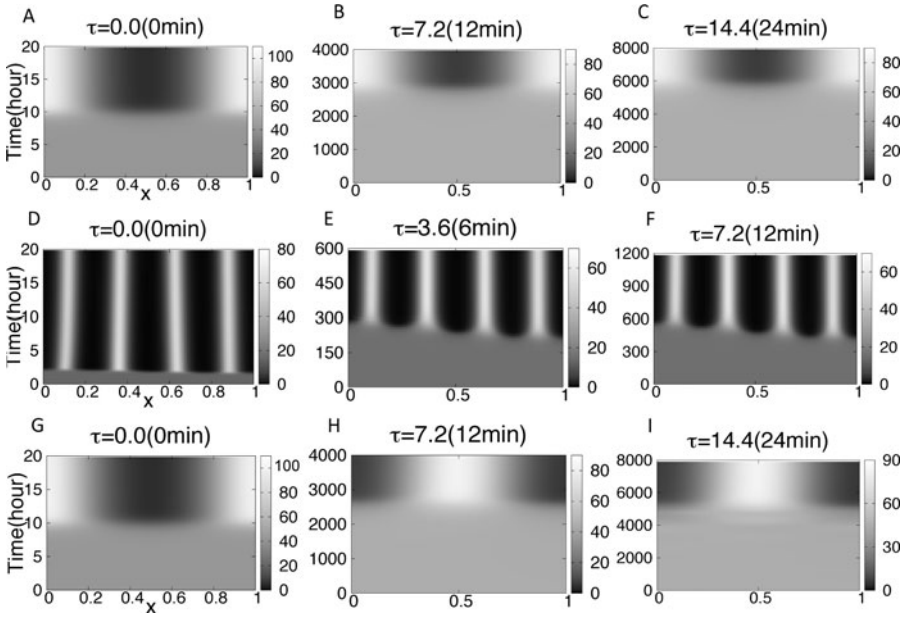

Fig. 8 Model II simulation results. The greyscale represents the non-dimensionalised concentration of the activator, the *horizontal axis* is the non-dimensionalised spatial coordinate and the *vertical axis* is time, which has been rescaled to units of hours. In the *first row*, parameter set II in Table 1 is used with initial conditions IC1, as given by Eq. (16), with $E_a = 1.25\text{e}{-}03$ and $E_b = 6\text{e}{-}03$. In the *second row*, parameter set III of Table 2 is used for the same initial conditions as the *first row*. In the final row parameter, set II in Table 1 is used once more, though now with the IC2 initial conditions of Eq. (17) with $E_a = 1.25\text{e}{-}03$, $E_b = 6\text{e}{-}03$ and $\delta = 2.5\text{e}{-}03$.

3.2.1. Model I results

Results for Model I are depicted in Figs. 5, 6 and there are a number of noteworthy observations from these simulations. First of all, as the time delay is increased even slightly the emergent pattern can fundamentally change, as illustrated by a comparison of Figs. 5D, E, and Figs. 6A, B. As the time delay is increased further, oscillatory patterns form as can be seen by comparing Figs. 5A, C, or Figs. 5D, F, or Figs. 6D, E. As the time delay is increased even further, all spatial heterogeneity can be lost, with temporal oscillations emerging, as illustrated by Fig. 6F. Note that for the scales considered, oscillatory behaviour is predicted to occur at time delays that are either less than, or the same order of magnitude as, the smallest estimates of gene expression time delays (Lewis, 2003; Tennyson et al., 1995).

The first rows of Figs. 5 and 6 differ from the second rows of the respective figures in the choice of initial conditions. Comparing these plots illustrates an observed trend that time delays can exacerbate pattern sensitivity to initial conditions. In addition, contrasting Figs. 5A, B we see that a six minute time delay results in a six hour patterning lag, illustrating the general prediction that gene expression time delays have a profound and amplified effect on the temporal control of patterning.

Finally note that once temporal oscillations occur, there is often an extraordinary loss of control of activator production, with an effective model break-down, and predictions

of extreme activator concentrations, as depicted in Figs. 6C, F. As the activator and inhibitor are in phase, this is not due to the denominator in the activator induced activator production term, U^2/V, as verified by replacing the denominator via $V \to \epsilon + V$ with $1 \gg \epsilon \gg 1e{-}03$. Formulating the gene expression delay model with this regularisation does not prevent the activator blow-up (results not shown). Thus, we have the observation that the activator blow up is not due to the effective absence of inhibitor but the failure of the inhibitor that is present in antagonising activator production.

3.2.2. Model I with the saturation of activator induced activator production

As activator levels can grow virtually uncontrollably during temporal oscillations in Model I, we also briefly consider the saturation of activator induced activator production. Typical model results are illustrated in Fig. 7 for the parameter set I of Table 1, where $\kappa > 0$. Note that as the gene expression time delay is increased the same behaviour emerges: temporal oscillations with spatial heterogeneity develop prior to spatially homogeneous oscillations, as depicted in Figs. 7B, D–F. The patterning lag is also very sensitive to the time delay, as illustrated by an inspection of Figs. 7A, B; furthermore, there is again an increased sensitivity to variations in the initial conditions as explicitly demonstrated by Figs. 7B, C which differ only in the choice of the initial conditions. However, as Figs. 7A–F also demonstrate the introduction of activator production saturation prevents an effective blow up in the amplitude of oscillations. This also allows one to explicitly observe that the initial bifurcation to symmetry breaking does not oscillate, though temporal oscillations subsequently emerge; see, Fig. 7D for example.

3.2.3. Model II, numerical results

In Fig. 8, we present results for numerical simulations of Model II given parameter set II of Table 1 with the initial conditions IC1 and IC2, as defined by Eqs. (16) and (17); results for parameter set III of Table 2 and initial conditions IC1 are also illustrated.

Firstly, note that temporal oscillations are not observed as the time delay is increased nor does the activator concentration blow up. One can also observe that even a small gene expression time delay can radically alter the final pattern, as illustrated by a comparison of Figs. 8G, H. However, the time delay exacerbates any sensitivity of the final pattern with respect to fluctuations in the initial condition, as can be seen by contrasting Fig. 8B, which utilises conditions IC1, with Fig. 8H, which uses condition IC2. Moreover, the most striking aspect of these results is the profound increase in the patterning lag for small increases in the gene expression time delay. For example, comparing Figs. 8G, H shows a patterning lag of around 2,500 hours for a 12 minute gene expression time delay; this is significantly greater than indicated by the linear analysis (see Fig. 4). We also briefly note that these qualitative features of Model II's behaviour appear to be generic; they are not altered for different parameter sets or the inclusion of activator induced saturation of activator production.

3.3. Further explorations of the sub-cellular kinetics: Models III and IV

Further to the illustration from Models I and II that differences in the sub-cellular interactions have a profound effect on the patterning dynamics, we briefly explore the correlation between oscillatory behaviour and the representation of signal transduction. We thus

Table 3 A summary of when temporal oscillations occur for the Gierer–Meinhardt model with gene expression dynamics and sufficiently large time delays according to whether the non-linear morphogen production reactions are instigated via ligand internalisation or via reversible ligand binding at the cell surface. In particular, inhibitor production and autocatalytic activator production proceed via signals induced by reversible ligand binding at the cell surface for Model I and via ligand internalisation for Model II. Model III assumes inhibitor production occurs via ligand internalisation with autocatalytic activator production induced via reversible ligand binding at the cell surface with the converse generating Model IV

Model	Reactions	Activator kinetics	Inhibitor kinetics	Oscillations
Model I	Reactions (6), (7)	$a - bu + \frac{u^2(x,t-\tau)}{v(x,t-\tau)}$	$u^2(x,t-\tau) - v$	Present
Model II	Reactions (10), (11)	$a - bu + 3\frac{u^2(x,t-\tau)}{v(x,t-\tau)} - 2\frac{u^2}{v} + c(u^2(x,t-\tau) - u^2)$	$u^2(x,t-\tau) - v$	Absent
Model III	Reactions (6), (11)	$a - bu + \frac{u^2(x,t-\tau)}{v(x,t-\tau)} + c(u^2(x,t-\tau) - u^2)$	$u^2(x,t-\tau) - v$	Absent
Model IV	Reactions (7), (10)	$a - bu + 3\frac{u^2(x,t-\tau)}{v(x,t-\tau)} - 2\frac{u^2}{v}$	$u^2(x,t-\tau) - v$	Present

consider Models III and IV. For the former, inhibitor production proceeds via ligand internalisation and autocatalytic activator production is induced by reversible ligand binding at the cell surface, with the converse for the latter. The results are summarised in Table 3. Note that temporal oscillations occur only with Models I and IV; thus, the cell surface induction of inhibitor production via reversible ligand binding appears to be driving the formation of temporal oscillations as the time delay is increased for the Gierer–Meinhardt system.

4. Discussion and conclusions

In this report, we have considered models of biological pattern initiation via interacting morphogens, focussing on the predictions of ubiquitous Gierer–Meinhardt model for different representation of gene expression time delays and sub-cellular dynamics. We typically focus on Model I and Model II. The former considers the induction of morphogen gene expression and production via reversible ligand binding at the cell surface; in distinct contrast, the latter presumes ligand internalisation is a pre-requisite for these processes.

We note that linear theory predictions are not reliable in general. Firstly, linear theory predicts the absence of a Hopf instability when the domain size is treated as a bifurcation parameter. Furthermore, the numerical simulations of Model I show that temporal oscillations readily emerge but not as part of the initial symmetry breaking event. Thus, the behaviour of the system at the initial symmetry breaking bifurcation is not generally representative of the long time dynamics of interacting morphogen models in the presence of time delays. Linear theory also significantly underestimates the timescales of the patterning lag in the presence of ligand internalisation, though the fact internalisation does greatly extend patterning times is correctly indicated. Nonetheless, this also clearly shows that in general linear theory cannot be relied upon to quantitatively predict the general features of temporal control of a delayed morphogen self-organisation model.

It is readily apparent that the introduction of gene expression time delays into the Gierer–Meinhardt model increases the sensitivity of the final pattern to fluctuations, such as in the initial conditions, which is illustrated by Figs. 8B, H. This sensitivity is frequently undesirable in development, leading some authors to question Turing patterning as a feasible biological mechanism (Bard and Lauder, 1974), though it has since been demonstrated that other mechanisms, such as domain growth, can greatly improve model robustness (Crampin et al., 1999). However, for the Schnakenberg system, the combination of domain growth and gene expression time delays can have severe effects on patterning, seen with neither mechanism in isolation (Gaffney and Monk, 2006). Consequently, an exploration of the influence of domain growth on patterning for pure kinetic models, such as Gierer and Meinhardt's, is merited so as to assess whether a lack of patterning robustness may re-emerge as a serious concern for modelling tightly regulated systems in the presence of gene expression time delays.

For Model I, which is the Gierer–Meinhardt system with the assumption that signal transduction occurs via reversible ligand binding at the cell surface, temporal oscillations are observed in the spatial patterning as the time delay is increased. Spatially homogeneous oscillations emerge as the time delay is increased further. Once such oscillations occur there is generally an unrealistic amplification of activator concentration, with levels exceeding seven to eight orders of magnitude greater than the homogeneous steady state. This blow up should be considered as a fundamental breakdown of the modelling framework, and thus adding gene expression time delays to a morphogen pattern initiation system can result in breakdown of the system in question. However, such a breakdown can be contingent on the sub-cellular dynamics; in particular it does not occur in models with ligand internalisation. Consequently, it will be difficult to classify which combinations of interaction kinetics and sub-cellular dynamics can lead to biologically reasonable predictions, though such explorations will clearly be insightful.

Consider Model II, which assumes ligand internalisation is present. Activator blow up does not occur nor do temporal oscillations but the patterning lag possesses an extreme sensitivity to the time delay; even small gene expression time delays have been observed to induce patterning lags greater than the time delay by four orders of magnitude. The resultant excessive patterning times would, at best, entail severe parameter space restrictions are required to apply such a model as a representation of developmental processes. Another serious consequence of these observations is the exquisite sensitivity to the smallest variations in the gene expression time delay, which would generate wildly different patterning times. A tight temporal control of pattern initiation is infeasible with such sensitivity and hence the relevance of a Gierer–Meinhardt model with gene expression time delays and ligand internalisation appears to be very severely restricted.

We return to Model I, which assumes reversible ligand binding occurs, but now with the saturation of activator induced activator production. This does not exhibit activator blow up during temporal oscillations, as previously seen in Model I, nor prohibitive sensitivity of the patterning lag with respect to the gene expression timescale, as observed in Model II. Nonetheless, spatially heterogeneous temporal oscillations are commonly predicted; these can induce patterning with appropriate cellular responses, such as thresholding or hysteresis, though this would be indicative of oscillatory mRNA profiles. This is not typically observed and hence temporal oscillation, spatially heterogeneous or otherwise, indicates a failure of self-organisation in these cellular models. Hence, initiating

spatially heterogeneous patterning with Model I, even with the saturation of activator induced activator production, requires the enforcement of substantial constraints to ensure the absence of temporal oscillations.

As summarised in Table 3, we observe temporal oscillations only if inhibitor production is initiated by reversible ligand binding at the cell surface rather than by ligand internalisation. The latter observation also reveals that the mechanism by which gene expression delays drives temporal oscillation is not a simple delayed negative feedback in the Gierer–Meinhardt model. In particular, the delayed negative feedback is present when inhibitor production is driven by ligand internalisation and yet temporal oscillations are absent. Consequently, future work exploring the mechanisms by which sub-cellular dynamics induce temporal oscillations in morphogen induced pattern formation may be fruitful in revealing constraints on feasible representations of signal transduction and protein synthesis during biological self-organisation.

The influence of gene expression time delays on Gierer–Meinhardt models is observed to be more severe than for Schnakenberg models on considering results from previous studies (Gaffney and Monk, 2006). With the latter, the main effect of gene expression delays given zero flux conditions on stationary domains is a substantially increased patterning lag, though not nearly to the extent seen in Model II. The fact predictions from Gierer–Meinhardt models on the inclusion of time delays include, for example effective blow ups and radical sensitivity highlights that once gene expression time delays are included; Turing pattern formation models do not exhibit qualitatively similar results. This contrasts observations in the absence of time delays (Murray, 1993) and more generally indicates that model behaviour on the inclusion of gene expression dynamics and other additional biology may provide a vehicle to distinguish between the numerous putative Turing pattern formation models.

Finally, for Gierer–Meinhardt kinetics we have observed a breakdown of the implicit, but fundamental, assumption underlying the Turing mechanism that one can represent morphogen dynamics by simply considering gene product interactions rather than the sub-cellular details. It is unclear whether the Gierer–Meinhardt system is pathological in this regard or if this is true more generally. Hence, there is also a clear need for multi-scale modelling considering the feedback between sub-cellular and gene expression dynamics with large scale pattern formation, so as to assess if and when the extra-cellular protein dynamics can be considered in isolation. Finally, these observations further emphasise that gene expression dynamics should not simply be ignored in models of cellular self-organisation via interacting morphogens.

Appendix A: Linear analysis

By substituting solutions of the form $A_n(t) = \exp(\lambda_n t)B_n$ into Eq. (19) where B_n is a constant vector, we obtain an eigenvalue equation as follows:

$$\begin{aligned}\varphi(\lambda_n) = \lambda_n^2 &+ \left\{n^2\pi^2 D\left(1+\epsilon^2\right) + \gamma(1-F_1) - \gamma G_1 e^{-\lambda_n \tau}\right\}\lambda_n \\ &+ \left(n^2\pi^2 D\epsilon^2 - \gamma F_1 - \gamma G_1 e^{-\lambda_n\tau}\right)\left(n^2\pi^2 D + \gamma\right) - \gamma^2(F_2+G_2)G_3 e^{-2\lambda_n\tau} \\ &= 0. \end{aligned} \tag{A.1}$$

The solutions of these equations for the eigenvalue λ_n determine the stability of the linearised equations corresponding to the delayed reaction diffusion system. However, as discussed in Section 4 and as also emphasised in Gaffney and Monk (2006) the predictions from linear theory are unreliable in general. Furthermore, non-standard analytical techniques are required to explore the above equations mathematically, due to the exponential dependence of the eigenvalue in the time delayed terms. Thus, a detailed mathematical analysis of Eqs. (A.1) is not considered though it is instructive to briefly explore the influence of a large time delay in the linearised system (19). In particular, we prove the following proposition for $F_1 \leq 0$ in these equations, which is satisfied by Models I and II and demonstrates that the patterning lag diverges with the time delay.

Proposition 1. *Assume* $F_1 \leq 0$. *Then for any* $\varepsilon > 0$ *and* $n \geq 0$ *we have* $\mathrm{Re}(\lambda_n(\tau)) < \varepsilon$ *for any sufficiently large* τ.

Proof: We can rewrite the statement above as $\limsup_{\tau\to\infty} \mathrm{Re}(\lambda_n(\tau)) < \varepsilon$. Suppose that $\limsup_{\tau\to\infty} \mathrm{Re}(\lambda_n(\tau)) \geq \varepsilon$ for some $\varepsilon > 0$.

We can easily see that $\limsup_{\tau\to\infty} |\lambda_n(\tau)| < \infty$. Assume the converse. Since $e^{-\lambda_n(\tau)\tau} \to 0$ as $\tau \to \infty$, we obtain the following contradiction from $\varphi(\lambda_n) = 0$:

$$1 = \lim_{\tau\to\infty} \frac{\lambda_n^2 + (n^2\pi^2 D(1+\epsilon^2) + \gamma(1-F_1) - \gamma G_1 e^{-\lambda_n\tau})\lambda_n}{\lambda_n^2}$$

$$= \lim_{\tau\to\infty} \frac{(n^2\pi^2 D\epsilon^2 - \gamma F_1)(n^2\pi^2 D + \gamma)}{\lambda_n^2} = 0.$$

Therefore, we have that $\lambda_n(\tau)$ converges to λ_n^∞, finite, as $\tau \to \infty$. From $\lim_{\tau\to\infty} \varphi(\lambda_n(\tau)) = \lim_{\tau\to\infty} 0 = 0$ and $\lim_{\tau\to\infty} |e^{-\lambda_n\tau}\lambda_n(\tau)| \leq \lim_{\tau\to\infty} e^{-\varepsilon\tau}|\lambda_n(\tau)| = 0$, we have

$$\left(\lambda_n^\infty\right)^2 + \left\{n^2\pi^2 D\left(1+\epsilon^2\right) + \gamma(1-F_1)\right\}\lambda_n^\infty + \left(n^2\pi^2 D\epsilon - \gamma F_1\right)\left(n^2\pi^2 D + \gamma\right) = 0.$$

Since $n^2\pi^2 D(1+\epsilon^2) + \gamma(1-F_1) > 0$ and $(n^2\pi^2 D\epsilon - \gamma F_1)(n^2\pi^2 D + \gamma) > 0$, λ_n^∞ has negative real parts, which contradicts the assumption that $\limsup_{\tau\to\infty} \mathrm{Re}(\lambda_n(\tau)) \geq \varepsilon$. Hence, $\limsup_{\tau\to\infty} \mathrm{Re}(\lambda_n(\tau)) < \varepsilon$ for arbitrary ε. □

Appendix B: Numerical methods for the reaction diffusion partial differential equations

On accounting for the time delay, the reaction diffusion systems that have been formulated in Sections 2.3.1–2.3.6 may be solved numerically via standard techniques; in the presented results the kinetics are considered explicitly with a fully implicit treatment of diffusive transport (Morton and Mayers, 1994). In particular, storing the history of the system for the duration of the time delay allows the generation of the kinetic terms within the numerical algorithm. A fully implicit treatment of the diffusive terms then generates a set of linear algebraic equations for the morphogen concentrations at each new timepoint, which may be solved using a choice of numerical techniques; we use an LU-decomposition. This numerical algorithm has been validated against the simulations of Gaffney and Monk (2006), which were generated from an independent code; it has also

been confirmed that refinements in the timestep and gridsize do not influence the results presented.

Acknowledgements

This publication is based on work supported in part by Award No. KUK-C1-013-04, made by King Abdullah University of Science and Technology (KAUST). SSL would like to thank Professor PK Maini and The Centre for Mathematical Biology for warm hospitality and a visiting position as well as gratefully acknowledging funding from the Japan Society for the Promotion of Science (JSPS Fellowship DC1).

References

Alberts, B., Johnson, A., Walter, P., Lewis, J., Raff, M., Roberts, K., 2002. Molecular Biology of the Cell, 5th edn. Garland, New York.

Baker, R.E., Gaffney, E.A., Maini, P.K., 2008. Partial differential equations for self-organization in cellular and developmental biology. Nonlinearity 21, R251–R290.

Bard, J., Lauder, I., 1974. How well does Turing's theory of morphogenesis work? J. Theor. Biol. 45, 501–531.

Baron, M., Aslam, H., Flasza, M., et al., 2002. Multiple levels of notch signal regulation (review). Mol. Membr. Biol. 19, 27–38.

Beguinot, L., Lyall, R.M., Willingham, M.C., Pastan, I., 1984. Down-regulation of the epidermal growth factor receptor in kb cells is due to receptor internalization and subsequent degradation in lysosomes. Proc. Natl. Acad. Sci. 81, 2384–2388.

Chen, Y., Schier, A., 2002. Lefty proteins are long-range inhibitors of squint-mediated nodal signaling. Curr. Biol. 12, 2124–2128.

Crampin, E.J., Gaffney, E.A., Maini, P.K., 1999. Reaction and diffusion on growing domains: Scenarios for robust pattern formation. Bull. Math. Biol. 61, 1093–1120.

Eldar, A., Dorfman, R., Weiss, D., Ashe, H., Shilo, B.Z., Barkai, N., 2002. Robustness of the BMP morphogen gradient in drosophila embryonic patterning. Nature 419, 304–308.

Entchev, E.V., Schwabedissen, A., Gonzalez-Gaitan, M., 2000. Gradient formation of the TGF-β homolog Dpp. Cell 103, 981–991.

Fischer, J.A., Eun, S.H., Doolan, B.T., 2006. Endocytosis, endosome trafficking, and the regulation of drosophila development. Annu. Rev. Cell Dev. Biol. 22, 181–206.

Gaffney, E.A., Monk, N.A.M., 2006. Gene expression time delays and Turing pattern formation systems. Bull. Math. Biol. 68, 99–130.

Gierer, A., Meinhardt, H., 1972. A theory of biological pattern formation. Kybernetik 12, 30–39.

Harris, M.P., Williamson, S., Fallon, J.F., Meinhardt, H., Prum, R.O., 2005. Molecular evidence for an activator–inhibitor mechanism in development of embryonic feather branching. Proc. Natl. Acad. Sci. USA 102(33), 11734–11739.

Iratini, R., Yan, Y.T., Chen, C., 2002. Drap1 gastrulation by the transcriptional corepressor inhibition of excess nodal signaling during mouse. Science 298, 1996–1999.

Jing, X.H., Zhou, S.M., Wang, W.Q., Chen, Y., 2006. Mechanisms underlying long- and short-range nodal signaling in zebrafish. Mech. Dev. 123, 388–394.

Juan, H., Hamada, H., 2001. Roles of nodal-lefty regulatory loops in embryonic patterning of vertebrates. Genes Cells 6, 923–930.

Jung, H.S., Francis-West, P.H., Widelitz, R.B., Jiang, T.X., Ting-Berreth, S., Tickle, C., Wolpert, L., Chuong, C.M., 1998. Local inhibitory action of BMPs and their relationships with activators in feather formation: Implications for periodic patterning. Dev. Biol. 196, 11–23.

Kimmel, C.B., Ballard, W.W., Kimmel, S.R., Ullmann, B., Schilling, T.F., 1995. Stages of embryonic development of the zebrafish. Dev. Dyn. 203, 253–310.

Koch, A.J., Meinhardt, H., 1994. Biological pattern formation: from basic mechanisms to complex structures. Rev. Mod. Phys. 66(4), 1481–1507.

Krezel, L.S., 2003. Vertebrate development: Taming the nodal waves. Curr. Biol. 13, R7–R9.
Lewis, J., 2003. Autoinhibition with transcriptional delay: A simple mechanism for the zebrafish somitogenesis oscillator. Curr. Biol. 13, 1398–1408.
Miura, T., Maini, P.K., 2004. Speed of pattern appearance in reaction-diffusion models: Implications in the pattern formation of limb bud mesenchyme cells. Bull. Math. Biol. 66, 627–649.
Miura, T., Shiota, K., 2000. Extracellular matrix environment influences chondrogenic pattern formation in limb bud micromass culture: Experimental verification of theoretical models. Anat. Rec. 258, 100–107.
Morton, K.W., Mayers, D.F., 1994. Numerical Solution of Partial Differential Equations. Cambridge University Press, Cambridge.
Murray, J.D., 1993. Mathematical Biology, 2nd edn. Springer, Berlin.
Page, K.M., Monk, N.A.M., Maini, P.K., 2007. Speed of reaction diffusion in embryogenesis. Phys. Rev. E 76, 011902.
Piddini, E., Vincent, J., 2003. Modulation of developmental signals by endocytosis: different means and many ends. Curr. Cell Biol. 15, 474–481.
Rauch, E.M., Millonas, M.M., 2004. The role of trans-membrane signal transduction in Turing-type cellular pattern formation. J. Theor. Biol. 226, 401–407.
Roy, C.L., Wrana, J.L., 2005. Clathrin- and nonclathrin-mediated endocytic regulation of cell signaling. Nat. Rev. Mol. Cell Biol. 6, 112–126.
Schier, A.F., 2003. Nodal signaling in verterbrate development. Rev. Cell Dev. Biol. 19, 589–621.
Schnakenberg, J., 1979. Simple chemical reaction systems with limit cycle behaviour. J. Theor. Biol. 81, 389–400.
Segel, L.A., Jackson, J.L., 1972. Dissipative structure. an explanation and an ecological example. J. Theor. Biol. 37, 545–559.
Sorkin, A., von Zastrow, M., 2002. Signal transduction and endocytosis: close encounters of many kinds. Nat. Rev. Mol. Cell Biol. 3, 600–614.
Stoscheck, C.M., Carpenter, G., 2002. Down-regulation of egf receptors: direct demonstration of receptor degradation in human fibroblasts. J. Cell Biol. 98, 1048–1053.
Tennyson, C.N., Klamut, H.J., Worton, R.G., 1995. The human dystrophin gene requires 16 hr to be transcribed and is contranscriptionally spliced. Nat. Gen. 9, 184–190.
Turing, A., 1952. The chemical basis of morphogenesis. Philos. Trans. R. Soc. Lond. B 237, 37–72.
Varea, C., Hernandez, D., Barrio, R.A., 2007. Soliton behaviour in a bistable reaction diffusion model. J. Math. Biol. 54, 797–813.
Veflingstad, S.R., Plahte, E., Monk, N.A.M., 2005. Effect of time delay on pattern formation: Competition between homogenisation and patterning. Physica D 207, 254–271.
Wells, A., Welsh, J.B., Lazar, C.S., Wiley, H.S., Gill, G.N., Rosenfeld, M.G., 1990. Ligand-induced transformation by a noninternalizing epidermal growth factor receptor. Science 247, 962–964.